



Alexandria University  
**Alexandria Engineering Journal**

[www.elsevier.com/locate/aej](http://www.elsevier.com/locate/aej)  
[www.sciencedirect.com](http://www.sciencedirect.com)



## ORIGINAL ARTICLE

# Unsteady viscous flow driven by the combined effects of peristalsis and electro-osmosis

Dharmendra Tripathi <sup>a,\*</sup>, Shashi Bhushan <sup>a</sup>, O. Anwar Bég <sup>b</sup>

<sup>a</sup> Department of Mechanical Engineering, Manipal University Jaipur, Rajasthan 303007, India

<sup>b</sup> Fluid Mechanics and Propulsion, Aeronautical and Mechanical Engineering, University of Salford, Newton Building, G77, The Crescent, Salford M54WT, England, UK

Received 16 February 2017; revised 14 May 2017; accepted 22 May 2017

## KEYWORDS

Peristalsis;  
 Electrokinetic phenomenon;  
 Trapping;  
 Electric double layer;  
 Analytical approach

**Abstract** Electrokinetic transport of fluids through microchannels by micro-pumping and micro-peristaltic pumping has stimulated considerable interest in biomedical engineering and other areas of medical technology. Deeper elucidation of the fluid dynamics of such transport requires the continuous need for more elegant mathematical models and numerical simulations, in parallel with laboratory investigations. In this article we therefore investigate analytically the unsteady viscous flow driven by the combined effects of peristalsis and electro-osmosis through microchannel. An integral number of waves propagating in the microchannel are considered as a model for transportation of fluid bolus along the channel length. Debye-Hückel linearization is employed to evaluate the potential function. Low Reynolds number and large wavelength approximations are employed. Closed-form solutions are derived for the non-dimensional boundary value problem. The computations demonstrate that magnitude of electric potential function is increased with a decrease in the thickness of the electrical double layer (EDL). Stronger electric field also decelerates the flow and decreases local wall shear stress. Hydrodynamic pressure is increased with EDL thickness whereas it is suppressed with electric field. Streamline visualization reveals that the quantity of trapped bolus is decreased with increase in EDL thickness and also with higher external electric field.

© 2017 Faculty of Engineering, Alexandria University. Production and hosting by Elsevier B.V. This is an open access article under the CC BY-NC-ND license (<http://creativecommons.org/licenses/by-nc-nd/4.0/>).

## 1. Introduction

Electro-osmosis refers to the transport of liquids by means of an applied electrical potential across a fluid conduit [1]. The

velocities associated with electro-osmosis are not controlled by the conduit size, provided that the electrical double layer (EDL) is significantly smaller than the characteristic length scale of the conduit e.g. channel. Electro-osmosis is a natural phenomenon in numerous medical and biological processes. It arises in botanical processes [2], canicular fluid flow in bone functioning [3] (interstitial fluid rich in ions), porous membranes [4], transport in the human skin [5], and dialysis mechanisms [6]. This phenomenon has been exploited in

\* Corresponding author.

E-mail address: [dharmtri@gmail.com](mailto:dharmtri@gmail.com) (D. Tripathi).

Peer review under responsibility of Faculty of Engineering, Alexandria University.

<http://dx.doi.org/10.1016/j.aej.2017.05.027>

1110-0168 © 2017 Faculty of Engineering, Alexandria University. Production and hosting by Elsevier B.V.

This is an open access article under the CC BY-NC-ND license (<http://creativecommons.org/licenses/by-nc-nd/4.0/>).

**Nomenclature**

$a$	half width at the inlet	$Q$	volumetric flow rate
$b$	wave amplitude	$\bar{Q}$	time-averaged volumetric flow rate
$c$	wave velocity		
$\bar{t}$	time		
$L$	channel length	<i>Greek symbols</i>	
$\bar{u}$	axial velocity	$\lambda$	wavelength
$\bar{p}$	pressure	$\bar{\xi}$	axial coordinate
$E_{\xi}$	electrokinetic body force	$\bar{\eta}$	transverse coordinate
$n^{+}$	number of densities of cations	$\rho$	fluid density
$n^{-}$	number of densities of anions	$\bar{v}$	transverse velocity
$e$	electronic charge	$\mu$	viscosity
$z$	charge balance	$\Phi$	electric potential
$K_B$	Boltzmann constant	$\rho_e$	density
$T$	average temperature of the electrolytic solution	$\varepsilon$	permittivity
$Re$	Reynolds number	$\delta$	wave number
$m$	electro-osmotic parameter	$\zeta$	zeta potential
$U_{HS}$	Helmholtz-Smoluchowski velocity	$\lambda_d$	Debye length
		$\tau_w$	local wall shear stress
		$\psi$	stream function

industrial separation techniques in biotechnology [7] and in particular in medical micro-pumps [8]. Micro-pumps have become popular in microfluidics, and electro-osmotic designs can generate significant pressures and flux without moving mechanical parts. In capillary electrophoresis devices, electro-osmotic pumping can achieve high efficiencies in capillaries lower than 100  $\mu\text{m}$  and this is beneficial to deployment in miniaturized chemical analysis systems. Electro-osmotic pumps offer similar advantages to electrohydrodynamic (EHD) pumps and traveling wave pumps since the electrical force imposed generates the pumping effect without any mechanical parts and thereby maintenance and other part-replacement issues can be mitigated. The ongoing refinement in electro-osmotic pump design has stimulated great interest in both experimental prototype testing and also computational and mathematical modelings. These two approaches have proved to be extremely complimentary in accelerating the arrival of next-generation electro-osmotic micro-pumps. Ngoma and Erchiqui [9] studied the dynamics of two immiscible fluids in a microchannel incorporating interfacial viscous shear stress, pressure gradient and electro-osmosis effects. They solved the Poisson–Boltzmann equation and modified Navier–Stokes equations for a steady fully-developed laminar flow and computed the electric potential, pressure difference, wall and interfacial zeta potentials. Zhao and Liao [10] considered non-isothermal electro-osmotic- and pressure-driven flow behavior in a straight microchannel, evaluating via a numerical finite difference method, the charge distribution density based on the nonlinear, two-dimensional Poisson–Boltzmann equation, and full Navier–Stokes equations with applied electrical potential field. They observed that maximum hydraulic head generated by the electro-osmotic force corresponds to an optimal dimensionless parameter which is the product of the inverse Debye length and the channel size.

The above studies considered the channel to be *non-deformable*. However a separate biological mechanism, *peristalsis*, has also been exploited in the development of high-efficiency and low-maintenance pumps in medical engineering.

Peristalsis, which arises in swallowing, digestive propulsion and phloem trans-location in plants, comprises an automatic periodic series of muscle contractions and relaxation, which can efficiently pump fluids, generally at low velocities (creeping flows). The literature on viscous peristaltic flows is extensive. Similarly in recent years many researchers have examined peristaltic magnetohydrodynamic flows from a theoretical standpoint i.e. where electromagnetic body force is present and the pumping fluid is electrically-conducting. Representative works in this regard are Tripathi and Bég [11] who also considered couple stress non-Newtonian effects. Kothandapani and Prakash [12] studied magnetized nanofluid peristalsis with radiative heat transfer. Akbar et al. [13] who considered magnetic induction and heat transfer effects in peristaltic pumping of carbon nanotube suspensions. Bhatti et al. [14] analyzed the endoscopic effects on blood flow in the presence of Titanium magneto-nanoparticles. They concluded that with increasing the magnitude of Sisko fluid parameter and Grashof number, the velocity of fluid flow alters. Same authors [15] again discussed the effects of variable magnetic field on peristaltic flow of viscoelastic fluid through non-uniform rectangular duct. They have reported that with increasing the magnetic field, the velocity of fluid flow diminishes. Most recently, Bhatti et al. [16] investigated the blood clotting effects on MHD peristaltic flow of viscoelastic nanofluids through annulus. They reported that the velocity reduces with increasing height of blood clot.

These studies however did not examine electric fields or electro-osmotic effects in peristaltic fluid dynamics. Apparently the first such investigation was communicated by Chakraborty [17] who developed analytical solutions to demonstrate that axial electric field can significantly elevate microfluidic transport rates in peristaltic flows in microtubes. He further elaborated on the modes of interaction between the electro-osmotic and peristaltic wave mechanisms, determining the pressure rise as a function of occlusion number, characteristic electro-osmotic velocity and the peristaltic wave speed. Tripathi et al. [18] further investigated electro-osmotic interaction

with peristaltic wave propagation in microtubes for a range of values of axial electric field. Goswami et al. [19] studied the electro-kinetically modulated peristaltic transport of power law fluids through a narrow deformable tube, observing that electro-osmosis has a more dramatic effect on pressure rise at lower occlusion values and furthermore that trapping is efficiently controlled via electric field and in fact is eliminated at sufficiently strong electrical field strengths as is the reflux phenomenon.

The combination of *peristaltic pumping* and *electro-osmosis* is attractive from the viewpoint of developing more effective micro-pumps [20,21]. In the present work we present a new hydrodynamic model to simulate the influence of external electric field and thickness of electric double layer (EDL) on peristaltic pumping of *viscous* fluids through a microchannel. We consider the more general case when an integral number of fluid boluses are propagating along the microchannel length. The model explored herein therefore aims to address the key questions of how to optimize the design of peristaltic electro-osmotic pumps via key parameters such as the thickness of Debye length and external electric field strength. The work is envisaged to shed further light on novel applications in microfluidic pumping processes and it is hoped that it will also stimulate other researchers to exploring this intriguing area of biomedical engineering.

**2. Mathematical model**

We consider transport in an electro-osmotic micro-pump with deformable channel walls. The *geometric model* for the electro-osmotic peristaltic pumping through a finite length ( $L$ ) channel, under an axial imposed electrical field,  $E_\xi$ , as illustrated in Fig. 1, is taken as follows:

$$\bar{h}(\bar{\xi}, \bar{t}) = a - b \cos^2 \frac{\pi}{\lambda} (\bar{\xi} - c\bar{t}) \quad \forall \bar{\xi} \in [0, L], \tag{1}$$

where  $\bar{h}, a, b, \lambda, \bar{\xi}, c, \bar{t}$  and  $L$  are the transverse displacement of the walls, the half width at the inlet, wave amplitude, wavelength, axial coordinate, wave velocity, time and channel length respectively. The electrical field vector retains only the axial electrical field component, and  $E_\xi$ , Electrical induced field is neglected since we are considering electrokinetic flow, not electrohydrodynamic (EHD) flow. In the latter electrical fields

are large enough to generate electrical induction phenomenon due to low thermal conductivity of fluids used in EHD. However they are not invoked in electrokinetic flows. The governing equations for unsteady, two-dimensional, viscous, incompressible flow with an axially-applied electrokinetic body force in the  $(\bar{\xi}, \bar{\eta})$  coordinate system, are given as follows:

$$\frac{\partial \bar{u}}{\partial \bar{\xi}} + \frac{\partial \bar{v}}{\partial \bar{\eta}} = 0, \tag{2}$$

$$\rho \left( \frac{\partial}{\partial \bar{t}} + \bar{u} \frac{\partial}{\partial \bar{\xi}} + \bar{v} \frac{\partial}{\partial \bar{\eta}} \right) \bar{u} = - \frac{\partial \bar{p}}{\partial \bar{\xi}} + \mu \left( \frac{\partial^2 \bar{u}}{\partial \bar{\xi}^2} + \frac{\partial^2 \bar{u}}{\partial \bar{\eta}^2} \right) + \bar{\rho}_e E_\xi, \tag{3}$$

where  $\rho, \bar{u}, \bar{v}, \bar{p}, \mu$ , and  $E_\xi$  denote the fluid density, axial velocity, transverse velocity, pressure, fluid viscosity, and axial electrical field (in the electrokinetic body force term). The Poisson equation for electric potential distribution is employed due to the presence of EDL in the micro-channel and is defined as follows:

$$\nabla^2 \bar{\Phi} = - \frac{\bar{\rho}_e}{\epsilon}, \tag{4}$$

Here  $\rho_e$  is the density of the total ionic charge and  $\epsilon$  is the permittivity. For a symmetric ( $z:z$ ) electrolyte, the density of the total ionic energy,  $\rho_e$  is given by,  $\rho_e = ez(n^+ - n^-)$ , in which  $n^+$  and  $n^-$  are the number of densities of cations and anions respectively. Nernst-Planck equation is defined to determine the potential distribution and describe the charge number density as follows:

$$\frac{\partial \bar{n}_\pm}{\partial \bar{t}} + (\mathbf{q} \cdot \nabla) \bar{n}_\pm = D \nabla^2 \bar{n}_\pm \pm \frac{Dze}{k_B T} (\nabla \cdot (\bar{n}_\pm \nabla \bar{\Phi})), \tag{5}$$

where  $D$  represents the diffusivity of the chemical species,  $k_B$  is the Boltzmann constant, and  $T$  is the average temperature of the electrolytic solution.

To facilitate analytical solutions it is advantageous to introduce a group of non-dimensional parameters

$$\begin{aligned} \xi &= \frac{\bar{\xi}}{\lambda}, & \eta &= \frac{\bar{\eta}}{a}, & t &= \frac{c\bar{t}}{\lambda}, & u &= \frac{\bar{u}}{c}, & v &= \frac{\bar{v}}{cd}, \\ \delta &= \frac{a}{\lambda}, & h &= \frac{\bar{h}}{a}, & \phi &= \frac{b}{a}, & p &= \frac{\bar{p}a^2}{\mu c \lambda}, \\ Re &= \frac{\rho c a}{\mu}, & \Phi &= \frac{\bar{\Phi}}{\zeta}, \end{aligned} \tag{6}$$

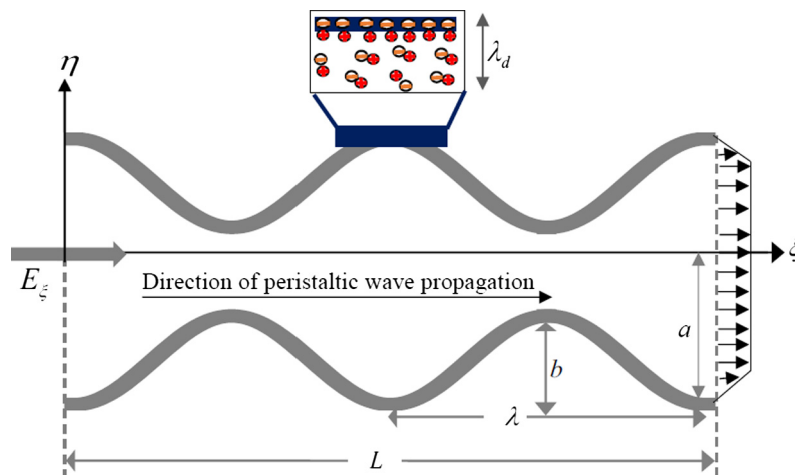


**Figure 1** Physical model for peristaltic wave propagation induced by electro-osmotic flow.

where  $\delta$  is wave number,  $Re$  is the Reynolds number. The potential function is non-dimensionalized with constant zeta potential ( $\zeta$ ). After non-dimensionalization, the nonlinear terms are appeared in the form of  $O(Pe\delta^2)$ , where  $Pe = ReSc$  represents the ionic Peclet number and  $Sc = \mu/\rho_f D$  denotes the Schmidt number. Using the limitations  $Re, Pe, \delta \ll 1$ , the Poisson equation is obtained as follows:

$$\frac{\partial^2 \Phi}{\partial y^2} = -\kappa^2 \left( \frac{n_+ - n_-}{2} \right) \tag{7}$$

and Nernst Planck equation is simplified to:

$$0 = \frac{\partial^2 n_{\pm}}{\partial y^2} \pm \frac{\partial}{\partial y} \left( n_{\pm} \frac{\partial \Phi}{\partial y} \right), \tag{8}$$

subjected to boundary conditions  $n_{\pm} = 1$  at  $\Phi = 0$  and  $\partial n_{\pm} / \partial y = 0$  where  $\partial \Phi / \partial y = 0$  (bulk conditions). These yield:

$$n_{\pm} = e^{\mp \Phi}. \tag{9}$$

Using Eqs. (7) and (9), the Poisson–Boltzmann paradigm is obtained as follows:

$$\frac{\partial^2 \Phi}{\partial y^2} = m^2 \sinh(\Phi). \tag{10}$$

where  $m = aez \sqrt{\frac{2n_0}{\epsilon K_B T}} = \frac{a}{\lambda_d}$ , is known as the electro-osmotic parameter,  $\lambda_d$  is Debye length or characteristic thickness of the electrical double layer (EDL). The Poisson–Boltzmann equation for zeta potential  $\zeta < 25$  mV (Debye–Hückel linearization i.e.  $\sinh(\Phi) \approx \Phi$ ), is expressed as follows:

$$\frac{\partial^2 \Phi}{\partial y^2} = m^2 \Phi. \tag{11}$$

Employing the boundary conditions:  $\Phi_y(0) = 0$  and  $\Phi(h) = 1$ , the potential function is obtained as follows:

$$\Phi = \frac{\cosh(\kappa y)}{\cosh(\kappa h)}. \tag{12}$$

Implementing non-dimensional variables in Eqs. (2) and (3), lead to the following non-dimensional conservations equations:

$$\frac{\partial u}{\partial \xi} + \frac{\partial v}{\partial \eta} = 0, \tag{13}$$

$$Re\delta \left( \frac{\partial}{\partial t} + u \frac{\partial}{\partial \xi} + v \frac{\partial}{\partial \eta} \right) u = -\frac{\partial p}{\partial \xi} + \left( \delta^2 \frac{\partial^2 u}{\partial \xi^2} + \frac{\partial^2 u}{\partial \eta^2} \right) + m^2 \Phi U_{HS}, \tag{14}$$

where  $U_{HS} = -\frac{E_z \epsilon \zeta}{\mu c}$  is the Helmholtz-Smoluchowski velocity or maximum electro-osmotic velocity. Applying long wave length and low Reynolds number approximations, as is customary for peristaltic hydrodynamics [22,23] the above Eqs. (8) and (9) reduce to the following linearized group of coupled partial differential equations:

$$\frac{\partial u}{\partial \xi} + \frac{\partial v}{\partial \eta} = 0, \tag{15}$$

$$\frac{\partial p}{\partial \xi} = \frac{\partial^2 u}{\partial \eta^2} + m^2 U_{HS} \Phi, \tag{16}$$

The associated normalized boundary conditions are as follows:

$$\begin{aligned} \frac{\partial u}{\partial \eta} \Big|_{\eta=0} &= 0, \quad u|_{\eta=h} = 0, \quad v|_{\eta=0} = 0, \\ v|_{\eta=h} &= \frac{\partial h}{\partial t}, \quad p|_{\xi=0} = p_0 \text{ and } p|_{\xi=L} = p_L, \end{aligned} \tag{17}$$

The boundary value problem is completely defined by the Eqs. (15)–(17). An analytical solution is sought and is elaborated in due course. Although non-linearity has been eliminated from the present model, nevertheless important phenomena associated with peristaltic wave interaction and electro-osmotic transport can still be studied. This furthermore provides a reasonable benchmark for more sophisticated non-linear simulations with numerical methods.

### 3. Analytical solutions

Integrating Eq. (16) and using boundary conditions (17), the axial velocity is obtained as follows:

$$u = \frac{1}{2} \frac{\partial p}{\partial \xi} (\eta^2 - h^2) - U_{HS} \left\{ \frac{\cosh(m\eta)}{\cosh(mh)} - 1 \right\}. \tag{18}$$

Using Eq. (18) and boundary condition (17), the transverse velocity by virtue of the continuity (mass conservation) Eq. (15) is obtained as follows:

$$\begin{aligned} v &= -\frac{1}{6} \frac{\partial^2 p}{\partial \xi^2} (\eta^3 - 3\eta h^2) + \eta h \frac{\partial p}{\partial \xi} \frac{\partial h}{\partial \xi} - U_{HS} \sinh(m\eta) \\ &\quad \times \frac{\tanh(mh)}{\cosh(mh)} \frac{\partial h}{\partial \xi}. \end{aligned} \tag{19}$$

Using Eq. (19) and boundary conditions (17), the axial pressure gradient is determined as follows:

$$\frac{\partial p}{\partial \xi} = \frac{1}{h^3} \left[ G_0(t) + 3 \left\{ \int \frac{\partial h}{\partial t} d\xi + U_{HS} \left( h - \frac{\tanh(mh)}{m} \right) \right\} \right], \tag{20}$$

where  $G_0(t)$  is arbitrary function of  $t$  to be evaluated using the finite length boundary conditions (17). The pressure difference can be computed along the axial length by

$$\Delta p = p(\xi, t) - p(0, t) = \int_0^\xi \frac{\partial p}{\partial s} ds, \tag{21}$$

and  $G_0(t)$  is expressed as follows:

$$G_0(t) = \frac{(p_L - p_0) - 3 \int_0^L h^{-3} \left\{ \int \frac{\partial h}{\partial t} d\xi + U_{HS} \left( h - \frac{\tanh(mh)}{m} \right) \right\} d\xi}{\int_0^L h^{-3} d\xi}. \tag{22}$$

The local wall shear stress is defined following Li and Brasseur [24]:

$$\tau_w = \frac{\partial u}{\partial \eta} \Big|_{\eta=h} = \frac{\partial p}{\partial \xi} h - m U_{HS} \tanh(mh). \tag{23}$$

The volumetric flow rate is defined as follows:

$$Q(\xi, t) = \int_0^h u d\eta = -\frac{1}{3} \frac{\partial p}{\partial \xi} h^3 + U_{HS} \left( h - \frac{\tanh(mh)}{m} \right). \tag{24}$$

The transformations between a wave frame  $(\xi_w, \eta_w)$  moving with velocity ( $c$ ) and the fixed frame  $(\xi, \eta)$  are given by

$$\xi = \xi_w - ct, \quad \eta = \eta_w, \quad u = u_w + c, \quad v = v_w, \quad (25)$$

where  $(u_w, v_w)$  and  $(u, v)$  are the velocity components in the wave and fixed frame respectively.

The volumetric flow rate in the wave frame is given by

$$q_w = \int_0^h u_w d\eta_w = \int_0^h (u - 1) d\eta_w, \quad (26)$$

which, on integration, yields:

$$q_w = Q - h. \quad (27)$$

Averaging volumetric flow rate along one time period, we get

$$\bar{Q} = \int_0^1 Q dt = \int_0^1 (q_w + h) dt, \quad (28)$$

which, on integration, yields:

$$\bar{Q} = q_w + 1 - \phi/2 = Q + 1 - h - \phi/2. \quad (29)$$

Using Eq. (18), the stream function in the wave frame (obeying the Cauchy-Riemann equations,  $u_w = \frac{\partial \psi}{\partial \eta_w}$  and  $v_w = -\frac{\partial \psi}{\partial \xi_w}$ ) takes the form:

$$\psi = \frac{1}{6} \frac{\partial p}{\partial \xi_w} (\eta_w^3 - 3\eta_w h^2) - U_{HS} \left( \frac{\sinh(m\eta_w)}{m \cosh(mh)} - \eta_w \right) \quad (30)$$

All the above expressions will reduce to the corresponding expressions for peristaltic transport of viscous fluids through a finite length channel with  $U_{HS} = 0$ . Furthermore the special case of peristalsis in the presence of electrokinetic transport through a very thin electric double layer may be retrieved with  $m \rightarrow \infty$ .

#### 4. Numerical results and discussion

In this section, numerical results obtained based on the closed-form solutions presented earlier, via symbolic code computation (Mathematica software), are described. We consider the effects of characteristic thickness of electric double layer ( $\lambda_d \propto 1/m$ ) and external electric field ( $E_z \propto U_{HS}$ ) on electrical potential, axial velocity, pressure distribution, local wall shear stress and trapping and representative plots are illustrated through Figs. 2–8.

Fig. 2(a & b) depicts the electrical potential profiles i.e. potential function vs. transverse coordinate. Evidently the potential profile exhibits a consistently symmetric parabolic shape across the width of the micro-channel i.e. it is minimum at the origin and exhibits maximum values at the channel walls. Fig. 2(a) shows the effect of thickness of EDL ( $\lambda_d \propto 1/m$ ) on the potential profile and it is noticed that magnitude of potential function ( $\Phi$ ) is elevated with reducing the thickness of EDL i.e. with decreasing values of  $m$  ( $m$  has an inverse relationship with  $\lambda_d$ ).

In other words with greater values of the electro-osmotic parameter ( $m$ ) the electric potential is elevated. Since  $m = \frac{a}{\lambda_d}$ , the electro-osmotic parameter is inversely proportional to the  $\lambda_d$  i.e. Debye length or characteristic thickness of the electrical double layer (EDL). Reducing Debye length therefore results in increasing the electrical potential. Similar observations have been reported in electro-kinetic simulations by for example Saville [25]. The electrical potential diminishes with every increase in Debye length since a greater quantity of

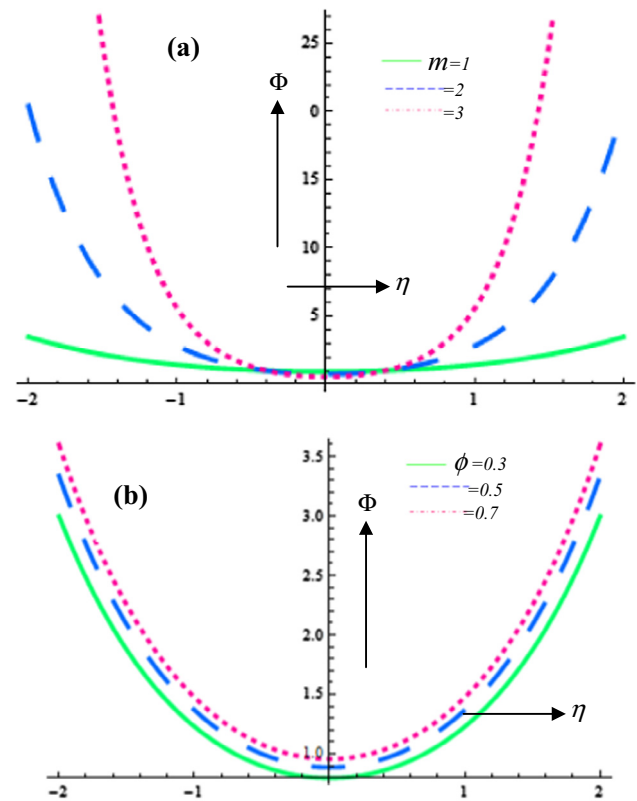
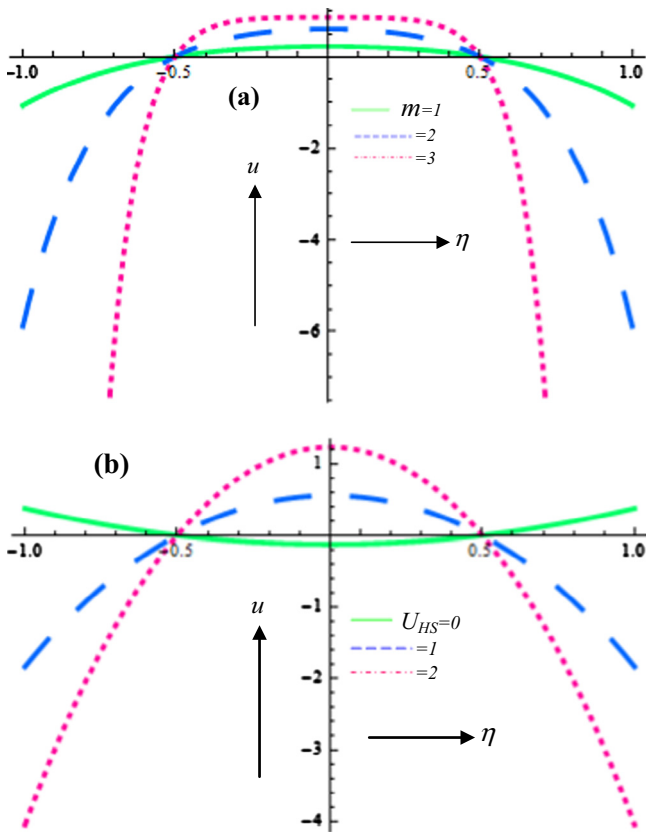


Figure 2 Electric potential profile at  $\xi = 1.0, t = 0$  for (a)  $\phi = 0.6$ , (b)  $m = 1$ .

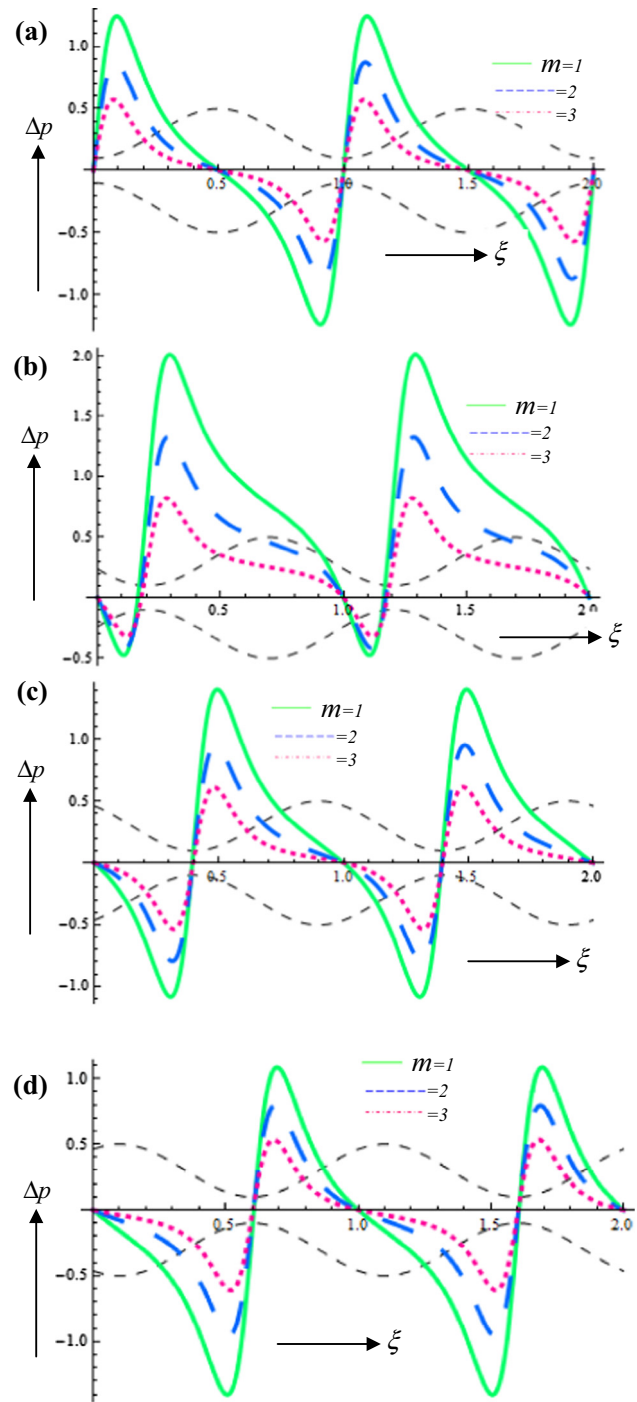
ions take the place of the counter ions as we progress away from the charged surface. Debye length is therefore a critical design parameter in controlling the electrical potential distribution. Fig. 2(b) depicts that the influence of amplitude of wave on potential profile. The snapshot depicted is at the initiation of flow i.e.  $t = 0$ . It is pointed out that potential function enhances with increasing the amplitude of the wave, indicating that the nature of the peristaltic wave can accentuate electrical potential in the micro-pump. Judicious selection of wave amplitude can therefore assist in elevating electrical potential magnitudes which in turn will encourage better performance of the micro-pump. These observations concur with the findings of for example Manz et al. [8] and also Chakraborty [17]. The potential distributions are, in both Fig. 2 (a and b), observed to be symmetrical parabolas with the minimum magnitudes arising at the channel centerline i.e. at the furthest location from the charged surface. The distributions in Fig. 2(a) are however sharper profiles whereas in Fig. 2(b) they are more dispersed.

Fig. 3(a & b) illustrates that the effects of EDL thickness and external electric field on velocity profile. Axial velocities consistently exhibit inverted parabolic profiles, demonstrating that as with purely viscous laminar channel flow –see Schlichting [26]- the maximum velocity arises at the channel centerline (i.e. at the greatest distance from the channel walls, where friction is a maximum). Fig. 3(a) depicts the effect of EDL thickness (indirectly again via the electro-osmotic parameter,  $m$ ) on velocity profile and a distinct displacement in profiles from parabolic to oblate parabolas (with the central plateau) which



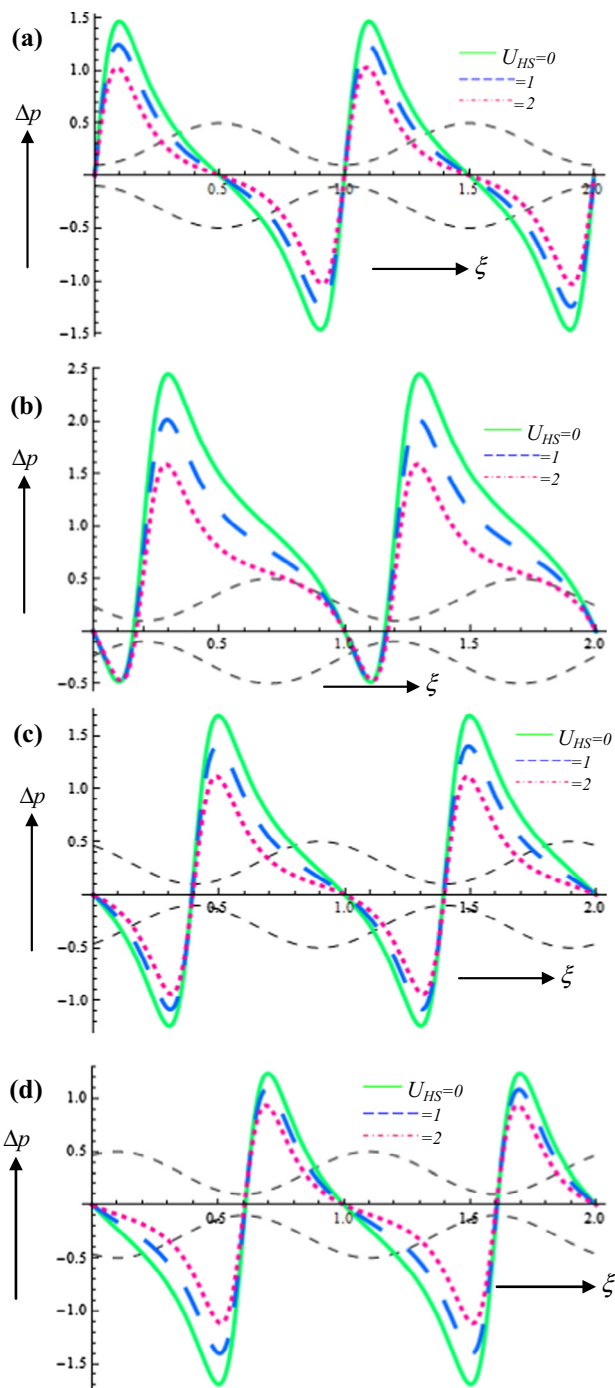
**Figure 3** Axial velocity vs. transverse coordinate at  $\phi = 0.5, \xi = 1.0, t = 0, \frac{\partial p}{\partial \xi} = 1$  for (a)  $U_{HS} = 1$  (b)  $m = 1$ .

are termed “trapezoidal” is witnessed, as electro-osmotic parameter ( $m$ ) is elevated i.e. as EDL thickness ( $\lambda_d$ ) is reduced. This shifting tendency is characteristic of the *electrokinetic* effect which modifies the velocity distribution from the Stokes’ flow profile (parabolic) to the electro-osmotic flow profile (flattened). This phenomenon has been reported in many studies including Gregersen et al. [27] and Bruus [28]. Fig. 3 (b) presents the different velocity profiles computed with and without external electric field. External electric field is simulated via the Helmholtz-Smoluchowski velocity or maximum electro-osmotic velocity,  $U_{HS} = -\frac{E_z \epsilon \zeta}{\mu c}$ . Evidently greater electric field (with all other parameters constrained) enhances the Helmholtz-Smoluchowski velocity. This in turn increases the electro-kinetic body force term, in the transformed linearized momentum Eq. (11) i.e.  $+m^2 U_{HS} \Phi$ . This body force is assistive to flow in the channel core region but inhibitive in the near-wall region, as elaborated by Probst [29], among others. The result is that with greater  $U_{HS}$  values the velocity is enhanced dramatically in the core region, as seen in Fig. 3b. Velocity profile is positively parabolic without external electric field whereas it is negatively parabolic (inverted) with external electric field. Hence the presence of increasing electrical field via greater  $U_{HS}$  values (1, 2) not only elevates velocities in the core region i.e. accelerates the core electro-osmotic flow, but also *reverses and significantly sharpens* the rather flat velocity profile without electro-kinetic effect ( $U_{HS} = 0$ ). The vertex of the parabolic velocity profile dramatically increases with increasing magnitude of external electric field. This trend is



**Figure 4** Pressure distribution along the length of channel at  $\phi = 0.8, l = 2, p_l = p_0 = 0, U_{HS} = 1$ . Color lines represent the pressure distribution for different values of Debye length at (a)  $t = 0$ , (b)  $t = 0.2$ , (c)  $t = 0.4$ , (d)  $t = 0.6$ . Black lines show the integral train wave propagation.

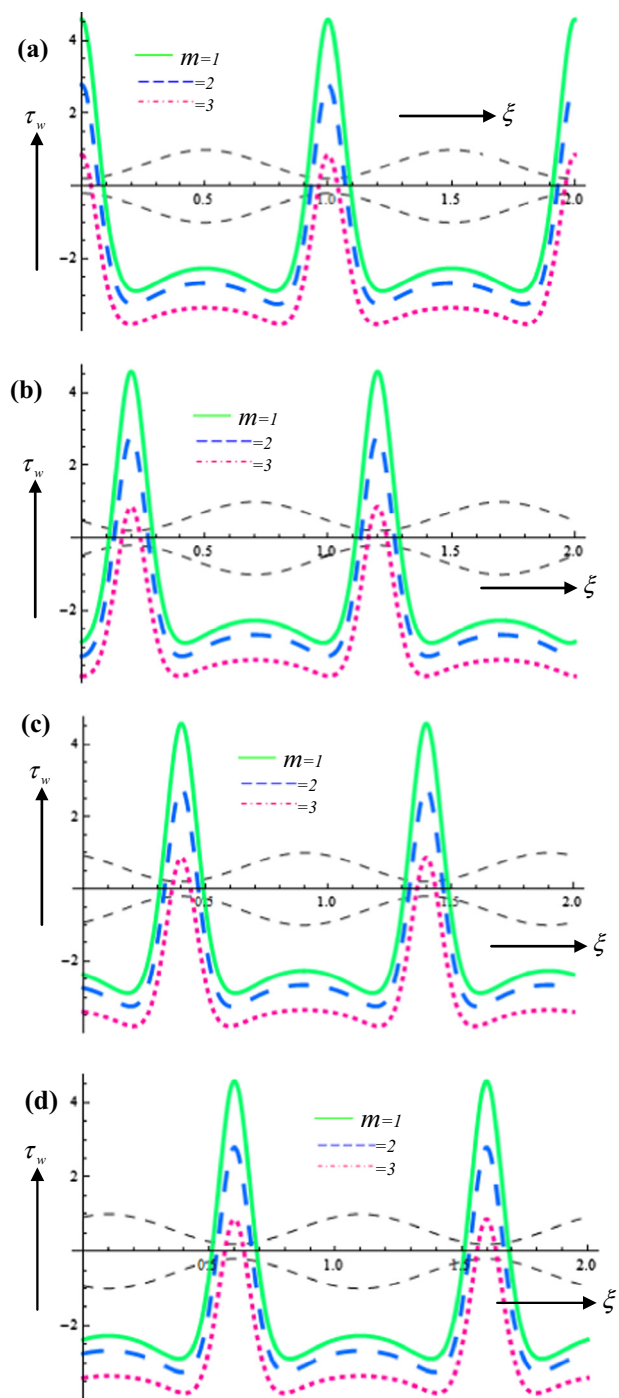
therefore consistent with the findings of Chakraborty [17] who has also demonstrated the beneficial nature of electric field to flow acceleration in electro-kinetics and has furthermore emphasized the great sensitivity of electro-osmotic flow to relatively low alterations in electric field strength. This has implications in practical electro-osmotic micro-pumps since



**Figure 5** Pressure distribution along the length of channel at  $\phi = 0.8, l = 2, p_l = p_0 = 0, m = 1$ . Color lines represent the pressure distribution for different values of Helmholtz-Smoluchowski velocity at (a)  $t = 0$ , (b)  $t = 0.2$ , (c)  $t = 0.4$ , (d)  $t = 0.6$ . Black lines show the integral train wave propagation.

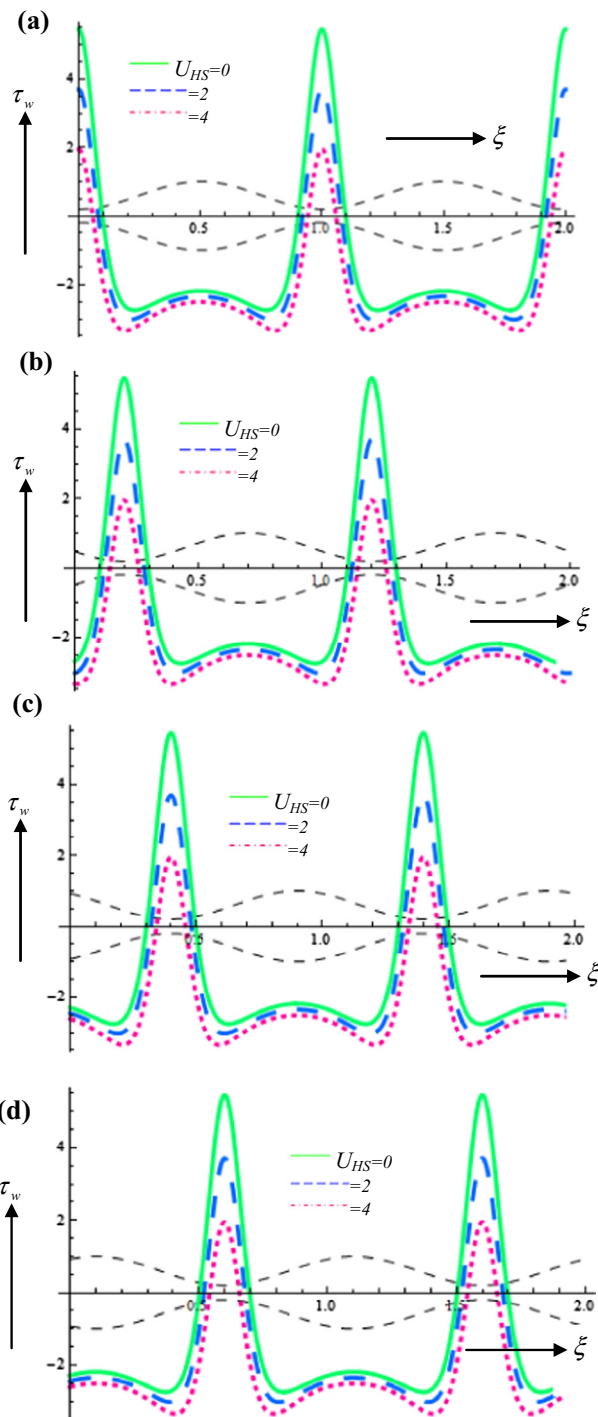
very good acceleration can be attained in the core flow with relatively minor adjustments in electric field, simultaneously reducing costs and addressing electromagnetic compatibility issues.

Fig. 4(a-d) is plotted for pressure distribution along the length of channel to evaluate the influence of EDL thickness and external electric field. To achieve more realistic simula-



**Figure 6** Local wall shear stress along the length of channel at  $\phi = 0.8, l = 2, p_l = p_0 = 0, U_{HS} = 1$ . Color lines represent the local wall shear stress for different values of inverse Debye length parameter at (a)  $t = 0$ , (b)  $t = 0.2$ , (c)  $t = 0.4$ , (d)  $t = 0.6$ . Black lines show the integral train wave propagation.

tions, in line with practical micro-pump behavior [30], an integral number of train waves are considered to propagate along the channel length i.e. *length of the channel* is considered as 2 times the wavelength of the *peristaltic wave*. The pressures at both ends of the channel are taken to be zero and four different steps of moving fluid bolus are visualized at different time



**Figure 7** Local wall shear stress along the length of channel at  $\phi = 0.8, l = 2, p_l = p_0 = 0, m = 1$ . Color lines represent the Local wall shear stress for different values of Helmholtz-Smoluchowski velocity at (a)  $t = 0$ , (b)  $t = 0.2$ , (c)  $t = 0.4$ , (d)  $t = 0.6$ . Black lines show the integral train wave propagation.

instants, namely  $t = 0, t = 0.2, t = 0.4$  and finally  $t = 0.6$ . It is apparent from inspection of the figures, that the pressure distribution is not uniform at the fully contracted walls. For example in Fig. 4(a), the pressure at the *first* contracted walls location is somewhat lower in magnitude than the subsequent

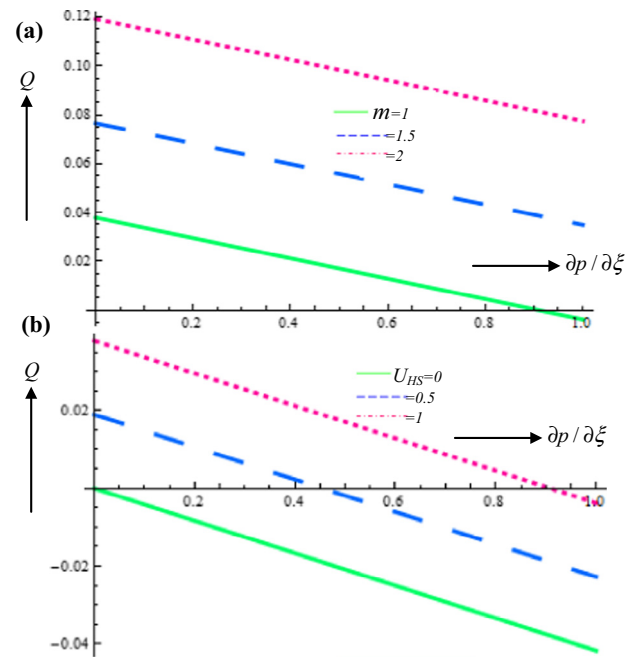


**Figure 8** Volumetric flow rate vs. pressure gradient at  $\phi = 0.5, t = 0$  for different values of (a) electro-osmotic parameter (inverse Debye length parameter) (b) Helmholtz-Smoluchowski velocity.

pressure computed at the second contracted walls. However the reverse pattern is observed in Fig. 4(b) and furthermore, in Fig. 4(c), pressure distribution is consistently uniform along the channel length. Conversely in Fig. 4(d), the pressure profiles are similar to Fig. 4a but the values are opposite i.e. wherever peaks and troughs arise in Fig. 4(a) the contrary is the case in Fig. 4(d). Generally it is also observed that the pressure enhances with increasing the magnitude of EDL thickness. In other words, as the electro-osmotic parameter ( $m$ ) is decreased and simultaneously EDL thickness ( $\lambda_d$ ) is increased, the pressure magnitudes are boosted in the channel. Therefore pressure can be sustained in the micro-pump performance with stronger electro-osmotic effect, which concurs with the computations of Ngoma and Erchiqui [9], among others.

Fig. 5(a-d) presents pressure distribution along the length of channel to compute the effects of external electric field, again via the variation in Helmholtz-Smoluchowski velocity  $U_{HS} = -\frac{E_z \epsilon \zeta}{\mu c}$ . As this parameter is increased from 0 (purely viscous flow) through 1 to a maximum value of 2, the increase in electric field is observed to consistently reduce the pressure magnitudes. Distinct from the velocity distributions presented earlier, there is no significant shift in nature of the pressure distribution profile from the non-electrical to the electro-osmotic cases. Electrical field therefore physically lowers pressures and this also contributes to acceleration in the core region, as elaborated earlier. The magnitudes are also depleted weakly with axial distance and with progression of time. Effectively greater pressure is achieved for peristaltic pumping *without external electric field* and vice versa, and again this trend agrees with the earlier studies of Chakraborty [17]. The periodic nature of pressure profiles is clearly captured in Fig. 5(a-d), and is associated with the propagation of peristaltic waves.

Fig. 6(a–d) illustrates the response in local wall shear stress ( $\tau_w$ ) along the channel length to variation in electro-osmotic parameter ( $m$ ) and indirectly the Debye EDL thickness ( $\lambda_d$ ). The same conditions are imposed as in Fig. 4. Local wall shear stress distribution is uniform and exhibits the classical W-shape, identified even in non-electro-osmotic (purely viscous) peristaltic hydrodynamics. The maximum shear stress arises at fully contracted walls while it is minimum at fully relaxed walls. This is directly attributable to the maximum impedance being encountered by the flow at the fully contracted walls and the opposite behavior when the walls are fully relaxed. The constriction in the walls when fully contracted significantly inhibits the flow and this increases the shear resistance at the walls i.e. boosts local wall shear stress. Four steps of local shear stress distribution computed at different time instants show the continuous chronological progress of the shear stress distribution. It is also evident that the local wall shear stress is enhanced with increasing magnitude of EDL thickness i.e. lower values of electro-osmotic parameter ( $m$ ). Decreasing  $m$  is known to accelerate the flow which results in greater shearing effects at the channel walls i.e. higher local wall shear stresses.

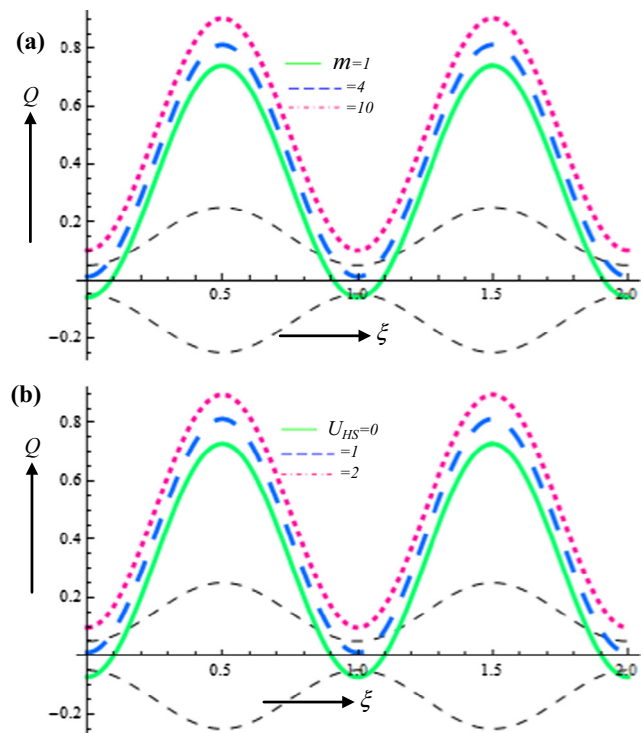
Fig. 7(a–d) depicts the impact of external electric field on local wall shear stress. It is depicted that local wall shear stress is suppressed for peristaltic pumping with increasing external electric field i.e. increasing  $U_{HS}$  (Helmholtz-Smoluchowski velocity or maximum electro-osmotic velocity is directly proportional to the electrical field strength,  $E_\xi$ ). This indicates that the flow is decelerated at the walls with greater electric field strength, an observation consistent with the velocity distributions described earlier in which flow acceleration was observed in the core flow, with simultaneous deceleration at the boundaries of the channel i.e. walls. The implication is that axial electric field can be deployed to accelerate and decelerate different zones in the flow. This allows designers to boost velocities in the core region and concurrently reduce them at the walls. Efforts in this regard have been communicated also by McKnight et al. [21].

Fig. 8(a, b) depicts the variation in volumetric flow rate ( $Q(\xi, t)$ ) with axial pressure gradient ( $\partial p/\partial \xi$ ) for different values of (a) electro-osmotic parameter (i.e.  $m = ae z \sqrt{\frac{2n_0}{\epsilon k_B T}} = \frac{a}{\lambda_d}$ ), and (b) Helmholtz-Smoluchowski velocity ( $U_{HS} = -\frac{E_\xi \epsilon \zeta}{\mu c}$ ) i.e. maximum electro-osmotic velocity. The inverse relationship between flow rate and pressure gradient is evident from inspection of both graphs. As pressure gradient increases, flow rate decreases. The decay clearly follows a linear pattern. Fig. 8(a) shows that increasing electro-osmotic parameter (i.e.  $m$ ) significantly elevates the volumetric flow rate. Magnitudes remain positive for both  $m = 1.5, 2$ ; however at higher pressure gradient volumetric flow is negative for  $m = 1$ . With increasing Helmholtz-Smoluchowski velocity ( $U_{HS}$ ), Fig. 8(b) demonstrates that there is also a significant enhancement in volumetric flow rate. However, whereas for  $U_{HS} = 1$  values are generally positive for all but very high values of the axial pressure gradient, for  $U_{HS} = 0.5$  they are initially positive and then assume negative values at intermediate values of the pressure gradient. For the case of vanishing electro-osmosis i.e.  $U_{HS} = 0$ , values are consistently negative for all pressure gradients. Furthermore it is noteworthy that magnitudes computed in Fig. 8(b) are substantially lower (an order of

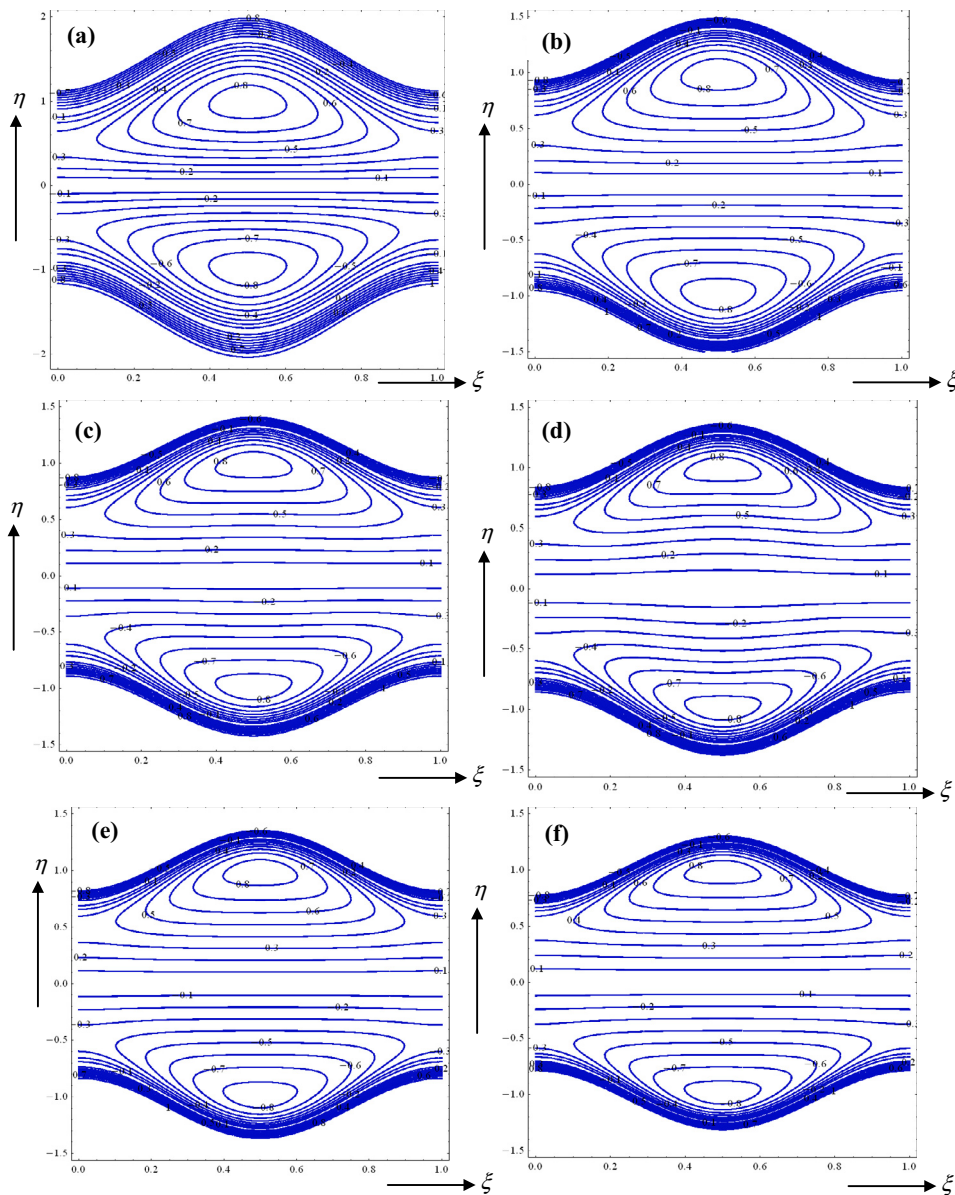
magnitude) than those in Fig. 8(a), at all values of axial pressure gradient.

Fig. 9(a and b) illustrates the evolution in volumetric flow rate ( $Q(\xi, t)$ ) with axial coordinate ( $\xi$ ) and with different values of (a) electro-osmotic parameter,  $m$  (inversely proportional to Debye length) and (b) Helmholtz-Smoluchowski velocity. In both plots well-dispersed periodic profiles are captured which illustrate clearly the sinusoidal nature of the peristaltic flow. Flow rates are observed to alternate i.e. attaining respective peaks then troughs. However the peaks are significantly greater in magnitude than the troughs as we progress from the channel entry ( $\xi = 0$ ) along the channel. With an increase in  $m$ , (Fig. 9a) there is a consistent enhancement in the volumetric flow rate. Effectively therefore greater electro-osmotic effect (smaller Debye length) markedly boosts flow rates. Fig. 9b shows that with increasing Helmholtz-Smoluchowski velocity there is also a marked elevation in flow rates. In other words greater axial electrical field enhances flow rate along the channel since the Helmholtz-Smoluchowski velocity is directly proportional to axial electrical field ( $U_{HS} = -\frac{E_\xi \epsilon \zeta}{\mu c}$ ).

Fig. 10(a–f) illustrates streamline distributions at prescribed values of amplitude and averaged volumetric flow rate  $\phi = 0.5, \bar{Q} = 0.6$  for different combinations of electro-osmotic parameter ( $m$ ) and also Helmholtz-Smoluchowski velocity ( $U_{HS}$ ). Via these two electro-kinetic parameters we can again examine the influence of EDL thickness and also external electric field on trapping phenomenon associated with peristaltic propulsion in the micro-channel. Trapping is an important phenomenon of peristaltic pumping in which the



**Figure 9** Volumetric flow rate along axial coordinate at  $\phi = 0.8, t = 0$  for different values of (a) electro-osmotic parameter (inverse Debye length parameter) (b) Helmholtz-Smoluchowski velocity.



**Figure 10** Streamlines at  $\varphi = 0.5, \bar{Q} = 0.6$ , (a)  $m = 5, U_{HS} = 0$ , (b)  $m = 5, U_{HS} = 1$ , (c)  $m = 5, U_{HS} = 2$ , (d)  $m = 5, U_{HS} = 3$ , (e)  $m = 8, U_{HS} = 1$ , (f)  $m = 10, U_{HS} = 1$ .

streamlines circulate and form a trapped bolus. It allows the determination of reflux characteristics and also vortex growth and circulation intensity in peristaltic flows. In Fig. 10(a–d), it is evident that the number of trapped boluses is markedly depleted with increasing external electric field i.e. increasing  $U_{HS}$  values. In particular significant distortion of streamlines arises in Fig. 8(a) at high transverse coordinate and intermediate axial coordinate values. Fig. 10(a, e & f) illustrates the impact of EDL thickness on trapping and reveal that the number of trapped bolus is also significantly reduced with increase in the thickness of EDL i.e. *decreasing* electro-osmotic parameter ( $m$ ).

## 5. Conclusions

Motivated by novel developments in electro-osmotic micro-pumps, a new mathematical model has been presented for

unsteady electro-osmotic peristaltic flow in a micro-channel, under the action of an axial electric field. Using creeping flow approximations, the electro-kinetic transport equations have been simplified via the Debye linearization and a non-dimensional, linearized boundary value problem derived. Closed-form solutions have been derived for axial velocity, electrical potential, local wall shear stress, axial pressure gradient and pressure difference. Numerical computations executed in symbolic software have been visualized to elucidate the influence of electro-kinetic, geometric and peristaltic wave parameters on the flow variables. The present computations have shown that:

- With increasing axial electrical field (i.e. increasing Helmholtz-Smoluchowski velocity) the axial flow is significantly accelerated in the core region of the micro-channel whereas it is decelerated at the micro-channel walls.

- With decreasing electro-osmotic parameter and increasing Debye length (electric double layer thickness, EDL), the axial flow is strongly accelerated in the core region whereas local wall shear stress is reduced.
- The number of trapped boluses is decreased with increasing external electric field i.e. increasing Helmholtz-Smoluchowski velocity values, and similarly it is reduced with increasing the thickness of EDL i.e. *decreasing* electro-osmotic parameter.
- With decreasing electro-osmotic parameter ( $m$ ) and simultaneous increase in EDL thickness, the pressure magnitudes are elevated. Similarly an *increase* in Helmholtz-Smoluchowski velocity and therefore axial electrical field, is found to reduce the pressure magnitudes.
- With increasing electrical field, axial flow is strongly accelerated in the core region. Furthermore velocity profile is positively parabolic without external electric field whereas it is negatively parabolic (inverted) with external electric field.
- The electrical potential is decreased with increasing EDL thickness i.e. decreasing electro-osmotic parameter.

## References

- [1] K.P. Tikhomolova, *Electro-Osmosis*, Ellis Horwood, London, 1993.
- [2] H. Ginsburg, Analysis of plant root electro-potentials, *J. Theor. Biol.* 37 (1972) 389–412.
- [3] V. Sansalone, J. Kaiser, S. Naili, T. Lemaire, Interstitial fluid flow within bone canaliculi and electro-chemo-mechanical features of the canalicular milieu, *Biomech. Model. Mechanobiol.* 12 (2013) 533–553.
- [4] E.A. Marshall, The osmotic flow of an electrolyte through a charged porous membrane, *J. Theor. Biol.* 66 (1977) 107–135.
- [5] S. Grimnes, Skin impedance and electro-osmosis in the human epidermis, *Med. Biol. Eng. Compu.* 21 (1983) 739–749.
- [6] T.A. Davis, Electrodialysis, in: M.C. Porter (Ed.), *Handbook of Industrial Membrane Technology*, Noyes Publications, New Jersey, USA, 1990.
- [7] V. Orsat, G.S.V. Raghavan, E.R. Norris, Food processing waste dewatering by electro-osmosis, *Can. Agric. Eng.* 38 (1996) 063–067.
- [8] A. Manz, C.S. Effenhauser, N. Burggraf, D.J. Harrison, K. Seiler, K. Fluri, *J. Micromech. Microeng.* 4 (1994) 257.
- [9] G.D. Ngoma, F. Erchiqui, Pressure gradient and electroosmotic effects on two immiscible fluids in a microchannel between two parallel plates, *J. Micromech. Microeng.* 16 (2005) 83–90.
- [10] T.S. Zhao, Q. Liao, Thermal effects on electro-osmotic pumping of liquids in microchannels, *J. Micromech. Microeng.* 12 (2002) 962.
- [11] D. Tripathi, O. Anwar Bég, Transient magneto-peristaltic flow of couple stress biofluids: a magneto-hydro-dynamical study on digestive transport phenomena, *Math. Biosci.* 246 (2013) 72–83.
- [12] M. Kothandapani, J. Prakash, Effect of radiation and magnetic field on peristaltic transport of nanofluids through a porous space in a tapered asymmetric channel, *J. Magn. Magn. Mater.* 378 (2015) 152–163.
- [13] N.S. Akbar, M. Raza, R. Ellahi, Influence of induced magnetic field and heat flux with the suspension of carbon nanotubes for the peristaltic flow in a permeable channel, *J. Magn. Magn. Mater.* 381 (2015) 405–415.
- [14] M.M. Bhatti, A. Zeeshan, R. Ellahi, Endoscope analysis on peristaltic blood flow of Sisko fluid with Titanium magneto-nanoparticles, *Comput. Biol. Med.* 78 (2016) 29–41.
- [15] M.M. Bhatti, A. Zeeshan, R. Ellahi, Simultaneous effects of coagulation and variable magnetic field on peristaltically induced motion of Jeffrey nanofluid containing gyrotactic microorganism, *Microvasc. Res.* 110 (2017) 32–42.
- [16] M.M. Bhatti, A. Zeeshan, R. Ellahi, Study of variable magnetic field on the peristaltic flow of Jeffrey fluid in a non-uniform rectangular duct having compliant walls, *J. Mol. Liq.* 222 (2016) 101–108.
- [17] S. Chakraborty, Augmentation of peristaltic microflows through electro-osmotic mechanisms, *J. Phys. D Appl. Phys.* 39 (2006) 5356–5363.
- [18] D. Tripathi, S. Bushan, O.A. Beg, Analytical study of electro-osmosis modulated capillary peristaltic hemodynamics, *J. Mech. Med. Biol.* 17 (2017) 1750052 (22 pages).
- [19] P. Goswami, J. Chakraborty, A. Bandopadhyay, S. Chakraborty, Electrokinetically modulated peristaltic transport of power-law fluids, *Microvasc. Res.* 103 (2015), <http://dx.doi.org/10.1016/j.mvr.2015.10.004>.
- [20] J. Goulpeau, D. Trouchet, A. Ajdari, P. Tabeling, Experimental study and modelling of polydimethylsiloxane peristaltic micropumps, *J. Appl. Phys.* 98 (2005) 044914.
- [21] T.E. McKnight, C.T. Culbertson, S.C. Jacobson, J.M. Ramsey, Electro-osmotically induced hydraulic pumping with integrated electrodes on microfluidic devices, *Anal. Chem.* 73 (2001) 4045–4049.
- [22] Y.C. Fung, C.S. Yih, Peristaltic transport, *ASME J. Appl. Mech.* 35 (1968) 669–675.
- [23] D. Tripathi and O. Anwar Bég, A study on peristaltic flow of nanofluids: application in drug delivery systems, *Int. J. Heat Mass Transfer* 70 (2014) 61–70.
- [24] M. Li, J.G. Brasseur, Non-steady peristaltic transport in finite-length tubes, *J. Fluid Mech.* 248 (1993) 129–151.
- [25] D.A. Saville, Electrokinetic effects with small particles, *Ann. Rev. Fluid Mech.* 9 (1977) 321–337.
- [26] H. Schlichting, *Boundary-Layer Theory*, sixth ed., McGraw-Hill, New York, 1979.
- [27] M.M. Gregersen, M.B. Andersen, G. Soni, C. Meinhardt, H. Bruus, Numerical analysis of finite Debye-length effects in induced-charge electro-osmosis, *Phys. Rev. E* 79 (2009) 066316.
- [28] H. Bruus, *Theoretical Microfluidics*, Oxford University Press, Oxford, 2008.
- [29] R.F. Probstein, *Physico-Chemical Hydrodynamics*, MacGraw-Hill, New York, 1989.
- [30] X. Zhang, Z. Chen, Y. Huang, A valve-less microfluidic peristaltic pumping method, *Biomicrofluidics* 9 (2015) 014118.